Study on tapered crossed subwavelength gratings by Fourier modal method*

Chen Xi(陈 熙)[a)†], Zhong Yuan(钟 源)[b)], Wang Qing(王 青)[a)], Zhang Ye-Jin(张冶金)[a)], and Chen Liang-Hui(陈良惠)[a)]

[a)] *Nano-Optoelectronics Laboratory, Institute of Semiconductors, Chinese Academy of Sciences, Beijing* 100083, *China*

[b)] *National Institute of Metrology, Beijing* 100013, *China*

(Received 17 December 2009; revised manuscript received 19 May 2010)

Fourier modal method incorporating staircase approximation is used to study tapered crossed subwavelength gratings in this paper. Three intuitive formulations of eigenvalue functions originating from the prototype are presented, and their convergences are compared through numerical calculation. One of them is found to be suitable in modeling the diffraction efficiency of the circular tapered crossed subwavelength gratings without high absorption, and staircase approximation is further proven valid for non-highly-absorptive tapered gratings. This approach is used to simulate the "moth-eye" antireflection surface on silicon, and the numerical result agrees well with the experimental one.

Keywords: tapered crossed subwavelength gratings, Fourier modal method, staircase approximation, eigenvalue functions

PACC: 4100H, 4225B, 4225F

1. Introduction

The fourier modal method (FMM), or rigorous coupled wave analysis (RCWA), is first proposed by Moharam and Gaylord to study the diffraction efficiency of one-dimensional (1D) surface-relief lamellar gratings.[1,2] During the past two decades, FMM has been intensively investigated. For 1D lamellar dielectric-metal gratings, the problem of slow convergence in TM mode has been solved by reformulating the eigenvalue functions, though it is unnecessary in TE mode.[3−8] Moreover, several authors have extended FMM to the lamellar crossed gratings.[9−14] However, FMM is unsuitable for the tapered gratings, whose permittivity in the longitudinal direction (normal to the grating surface) is not constant. Meanwhile there is a need to study the antireflection (AR) performance of the tapered crossed subwavelength gratings (TCSWGs), or the moth-eye structures.[15] The corneal nipple structures in the eyes of moth are graded-refractive-index structures in essence, which enhance the light sensitivity at night and reduce reflectance at daytime.[16] Inspired by the moth-eye principle, TCSWGs of semiconductors[17−20] patterned with a scale smaller than the wavelength of incident light, can greatly suppress the reflection over a broad spectrum, and has a potential application in photonic devices which need AR surface, such as light emitting diodes, solar cells, and photodetectors. As FMM is one of the simplest and most versatile approaches based on the rigorous solutions to the electromagnetic (EM) field of crossed gratings,[21] the tapered profiles of TCSWGs are treated as discretized sidewalls under staircase approximation so that it could be used.

The aim of this paper is to provide a detailed study on TCSWGs using FMM under staircase approximation. In Section 2, a formulation for the implementation of the FMM for the TCSWGs incorporating staircase approximation is presented, along with the prototype of eigenvalue functions. One of the key issues for modeling crossed gratings by FMM is to form proper eigenvalue functions, which are related to the shape and lattice type,[10−14,21−23] to achieve a fast convergence. For simplicity, only square-latticed TCSWGs with circular and rectangular shapes are discussed in this paper. Three intuitive formulations of eigenvalue equations originating from the prototype are presented and compared through numerical examples in Section 3. It has been proven that staircase

*Project supported by the National Natural Science Foundation of China (Grant No. 60636030).

†Corresponding author. E-mail: chenxi@semi.ac.cn

© 2010 Chinese Physical Society and IOP Publishing Ltd

approximation is not accurate for highly-absorptive gratings like metal ones, for it introduces local maxima at the edges of the discretized sidewalls, which requires greater truncated number to correctly represent the EM field, and leads to the deterioration in the convergence as the number of the divided slices increases.[24] However, what we aim at are the lossless and low-loss TCSWGs, and we will prove in Section 4 that the staircase approximation is valid in these cases. Based on the conclusions of Sections 3 and 4, a moth-eye structure is simulated, and the result is compared with the experimental one in Section 5.

2. Formulation of FMM incorporating staircase approximation

To model TCSWGs with FMM, the smoothed tapered profiles are approximated to be the staircase ones. The model is depicted in Figs. 1 and 2. A plane wave is incident from Region I to Region II at a polar angle θ, an azimuthal angle φ and a polarization angle ψ. The square-latticed TCSWGs with a depth of d are equally divided into L slices along the z direction. Every single slice is composed of biperiodic cells with vertical sidewalls, for which FMM could be utilised.

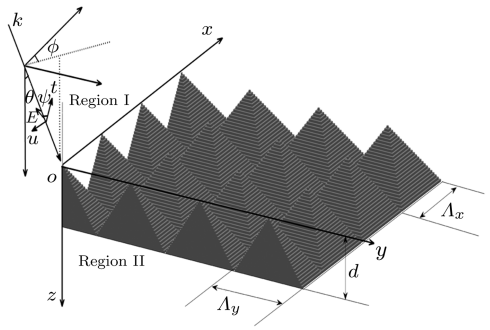


Fig. 1. Schematic of staircase approximation in TCSWGs.

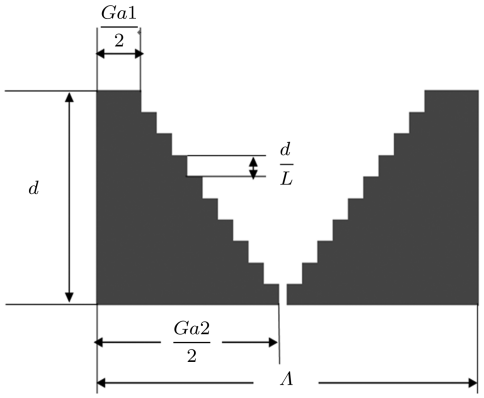


Fig. 2. Cross-sectioned view of TCSWGs in one period along x or y direction.

Figure 2 is the schematic of the cross-sectioned view of the tapered profile under staircase approximation. The variation of the profile is assumed to be linear along the z direction, with the widths of every cell along the x and y directions being the same. We introduce four parameters to describe the tapered profile: $Ga1, Ga2, ga1$ and $ga2$, which are defined as $\mathrm{ga1} = Ga1/\Lambda$, $ga2 = Ga2/\Lambda$. $ga1$ and $ga2$ are indeed the duty ratios of the top and bottom slices respectively. The notations are those used in Ref. [11]. Given $Ga1$, $Ga2$, d and L, the geometric parameters of each slice are defined, so are the permittivity harmonic coefficient $\varepsilon_{mn}^{(i)}$, and the inversed permittivity harmonic coefficient $\xi_{mn}^{(i)}$. The superscript i denotes the slice number the corresponding parameters belong to. M is defined as the truncated order of harmonic series in Fourier expansion. $E^{(i)}$ and $A^{(i)}$ are the matrices formed by $\varepsilon_{mn}^{(i)}$ and $\xi_{mn}^{(i)}$ respectively. I is the identity matrix, while K_x and K_y are the diagonal matrices. $\boldsymbol{S}^{(i)}$ and $\boldsymbol{U}^{(i)}$ are the electric and magnetic field vectors in the i-th slice. The eigenvalue functions of the i-th slice are

$$\begin{pmatrix} \dot{S}_y^{(i)} \\ \dot{S}_x^{(i)} \\ \dot{U}_y^{(i)} \\ \dot{U}_x^{(i)} \end{pmatrix} = \begin{pmatrix} 0 & 0 & K_y A^{(i)} K_x & I - K_y A^{(i)} K_x \\ 0 & 0 & K_x A^{(i)} K_y - I & -K_x A^{(i)} K_y \\ K_x K_y & E^{(i)} - K_y^2 & 0 & 0 \\ K_x^2 - E^{(i)} & -K_x K_y & 0 & 0 \end{pmatrix} \begin{pmatrix} S_y^{(i)} \\ S_x^{(i)} \\ U_y^{(i)} \\ U_x^{(i)} \end{pmatrix}, \tag{1}$$

The notation of dot $\cdot$ at the top of S and U denotes the first-order derivative with respect to $k_0 z$, where k_0 is the wave number in vacuum. Readers who are interested in the achievement of Eq. (1) can refer to Ref. [25], which gives in detail about the implementation of FMM for the lamellar crossed gratings with rectangular shape. The relevant eigenvalues and eigenvectors can be gained by solving the eigenvalue functions. The solutions of each slice are combined with their boundary conditions in each inter-

face, so that R and T as well as the EM field distribution inside the slices are solved simultaneously. Scattering matrix (S-matrix) method[26,27] is usually utilized, while we prefer the enhanced transmittance matrix approach,[28] which we found was more convenient to be incorporated into our computer codes (in Matlab). R and T denote the normalized power of total reflectance and transmission respectively, and absorption is given by $1 - R - T$.

The same checkerboard gratings in Ref. [9] are simulated by our approach: use $ga1 = ga2$, equation (1) as eigenvalue functions. The results are close to those in Table 1 of Ref. [9], and they keep constant regardless of the values of L. Furthermore, the approach is examined by the following criteria: (a) for the dielectric TCSWGs, "$R + T = 1$" is always met even though M varies; (b) the results gradually converge to a certain value as M increases; (c) by setting ψ as 90° and 0°, which stand for s and p polarization respectively, the results are exactly the same in normal incidence. Our simulated results meet the three criteria. Further numerical proofs can be found in the following sections.

3. Comparison of the three types of eigenvalue functions

In Eq. (1), the eigen-matrix is composed of two submatrices in the upper right and lower left corners, which are denoted as Ω_1 and Ω_2 respectively. The three types of eigenvalue functions are:

Formulation 1 ($F1$): $[E^{(i)}]^{-1}$ instead of $A^{(i)}$ is used in Ω_1;

Formulation 2 ($F2$): $[E^{(i)}]^{-1}$ instead of $A^{(i)}$ is used in Ω_1, $\alpha[A^{(i)}]^{-1} + (1-\alpha)E^{(i)}$ instead of $E^{(i)}$ is used in Ω_2 and $\alpha = f_x\Lambda_x/(f_x\Lambda_x + f_y\Lambda_y)$, where f_x and f_y denote the duty ratios along x and y directions respectively;

Formulation 3 ($F3$): $[E^{(i)}]^{-1}$ instead of $A^{(i)}$ is used in Ω_1, and $[A^{(i)}]^{-1}$ instead of $E^{(i)}$ is used in Ω_2.

TCSWGs here are assumed to be made of silicon (region II), and the simulated parameters are listed as follows: $d = 0.35$ μm, $\Lambda = \Lambda_x = \Lambda_y = 0.15$ μm, $L = 25$, $ga1 = 0$, $ga2 = 1$, $\theta = 0°$, $\varphi = 0°$, $\psi = 0°$. Setting period = 0.15 μm is to fulfill the demand of being smaller than the solar spectra. Two shapes, rectangle and circle, are calculated respectively. For silicon, the complex refractive index is 5.442–i2.989 when $\lambda = 0.3502$ μm, and 3.688–i0.006 when $\lambda = 0.8051$ μm.[29] The former can be taken as low-loss material, while the latter as the roughly lossless one.

With $\lambda = 0.3502$ μm and $d = 0.35$ μm, absorption is dominant as compared to R and T, so we choose it to compare the convergence for different shapes. Figures 3(a) and 3(b) show absorption as a function of M for rectangular and circular shapes respectively.

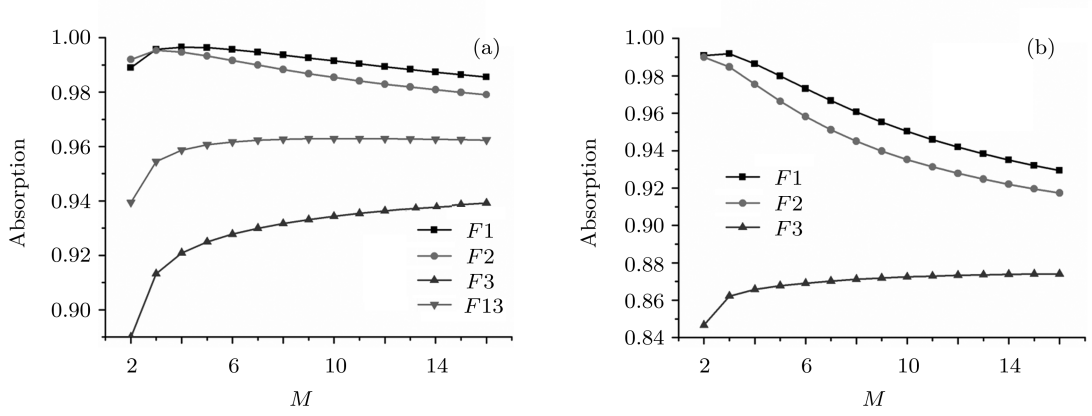


Fig. 3. Convergence of absorption versus M: TCSWGs of silicon, $\lambda = 0.3502$ μm, (a) rectangular shape; (b) circular shape.

For $\lambda = 0.8051$ μm, absorption is very small. As $\lambda/(n_{\rm air}\Lambda) > 2$, there is only R_{00} among back diffractions, so it is chosen here to compare the convergence. Figures 4(a) and 4(b) are the normalized R_{00} as a function of M for rectangular and circular shapes respectively.

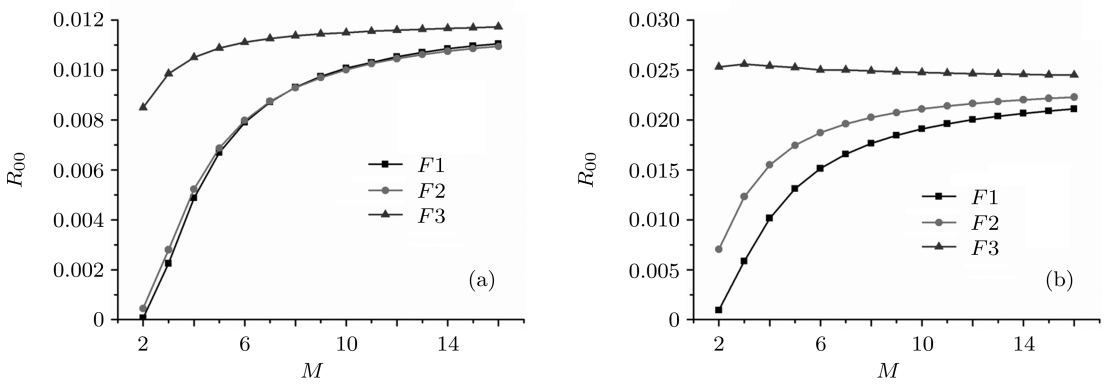


Fig. 4. Convergence of R_{00} versus M: TCSWGs of silicon, $\lambda = 0.8051$ μm, (a) rectangular shape; (b) circular shape.

From Figs. 3 and 4, as other authors have reported,[5,6,11] we observed that eigenvalue functions in proper formulation have a crucial influence on the convergence. The convergence problem primarily arises from a product of two periodic functions both of which are expanded into Fourier series. To be realized in numerical calculation, the Fourier series which should have been in infinite order is truncated by a limited order of M. Thus the larger the M is, the more accurate the results will be. However, a larger M also means that much more time and more computer memory are needed for calculation. The situation becomes more severe when dealing with the crossed gratings. For example, we cannot solve the case of $M > 16$ due to out of memory of our computer. Li[6] gave his solution to this problem with a solid mathematical foundation. Given periodic functions $f(x)$ and $g(x)$, the product of them is $h(x) = f(x)g(x)$. As $h(x)$ needs to be Fourier factorized in every x position, Li concluded that the following theorem should be obeyed: (i) if $f(x)$ and $g(x)$ have no concurrent jump discontinuities, $h(x)$ can be Fourier factorized by Laurent rule; (ii) if $f(x)$ and $g(x)$ have only complementary jump discontinuities, inversed rule rather than Laurent rule should be used. By following Li's theorem, the convergence in TM mode for 1D gratings has been remarkably improved. Unfortunately, the 2D situation is more complex than the 1D one.

We transform Eq. (1) back to its more original form

$$\frac{\partial E_y}{\partial z} = \frac{\partial}{\partial y}\left[\frac{1}{\mathrm{j}\omega\varepsilon}\left(\frac{\partial H_y}{\partial x} - \frac{\partial H_x}{\partial y}\right)\right] + \mathrm{j}\omega\mu_0 H_x, \quad (2)$$

$$\frac{\partial E_x}{\partial z} = \frac{\partial}{\partial x}\left[\frac{1}{\mathrm{j}\omega\varepsilon}\left(\frac{\partial H_y}{\partial x} - \frac{\partial H_x}{\partial y}\right)\right] - \mathrm{j}\omega\mu_0 H_y, \quad (3)$$

$$\frac{\partial H_y}{\partial z} = \frac{\partial}{\partial y}\left[-\frac{1}{\mathrm{j}\omega\mu_0}\left(\frac{\partial E_y}{\partial x} - \frac{\partial E_x}{\partial y}\right)\right] - \mathrm{j}\omega\varepsilon E_x, \quad (4)$$

$$\frac{\partial H_x}{\partial z} = \frac{\partial}{\partial x}\left[-\frac{1}{\mathrm{j}\omega\mu_0}\left(\frac{\partial E_y}{\partial x} - \frac{\partial E_x}{\partial y}\right)\right] + \mathrm{j}\omega\varepsilon E_y. \quad (5)$$

The specific shapes of crossed gratings, rectangular and circular, are placed in the 2D Cartesian coordinate system as shown in Fig. 5. For rectangular shape, equations (2) and (3) indicate that $(1/\mathrm{j}\omega\varepsilon)\,(\partial H_y/\partial x - \partial H_x/\partial y)$ is continuous along x and y directions, as its first-order derivatives with respect to x and y exist. However, $(\partial H_y/\partial x - \partial H_x/\partial y)$ is not continuous. The reason is that it is equal to $\mathrm{j}\omega\varepsilon E_z$, while εE_z is discontinuous along the x and y directions as shown in Fig. 5. There must be complementary jump discontinuity along x and y directions. Following Li's theorem, $[\varepsilon_{mn}]^{-1}$ rather than $[\xi_{mn}]$, regarded as inversed rule, should be used to form the correct Fourier factorisation in Ω_1. Inversed rule can also be easily found to be valid in Ω_1 of circular crossed gratings for the same reason. The same analysis is carried out in Ω_2. For rectangular ones, εE_x on the right-hand side of Eq. (4) is continuous along x and discontinuous along y direction, while ε is discontinuous along x and y directions. Accordingly, inversed rule is valid in x direction, and Laurent rule valid in y direction, and *vice versa* for Eq. (5). The dependence of ε (or ξ) on x and y cannot be separated from each other, so neither Laurent nor inversed rule can be used in Eqs. (4) and (5). Circular ones also encounter the same problem, for the normal and tangential directions in an arbitrary position of the circular interface, as denoted by u and t respectively in Fig. 5, are not always parallel to x or y direction. To establish optimal eigenvalue functions, Li's theorem should be followed to have Ω_1 and Ω_2 Fourier factorized correctly, meanwhile the exact shape and the lattice type should be taken into account. Many papers have been presented to address this issue,[10−14,21−23] especially

for the highly absorptive gratings. Still, it is difficult to find a versatile formulation to model crossed gratings of arbitrary shape, and those approaches are far more complex. Although the three types of eigenvalue functions proposed in this paper are intuitive, they are obtained directly from the prototype and much easier to achieve and to be incorporated into the computer codes. For rectangular crossed gratings, $F1$, $F2$, and $F3$ all choose the correct form in Ω_1, but they are not valid in Ω_2 in view of truncated Fourier series. In Ω_2, $F1$ obeys Laurent rule, and $F3$ inversed rule. As for $F2$, it is proposed by Lalanne[11] to model crossed gratings of rectangular shape, and $\alpha = 0.5$ is introduced to weigh the relative strengths of $[\varepsilon_{mn}]^{-1}$ and $[\xi_{mn}]$, which indeed can be regarded as a trade-off between the Laurent and inversed rules for both the x and y directions. The convergences of $F1$, $F2$, and $F3$ are not very good as shown in Fig. 3(a), where the curves of all the three gradually approach to the intermediate zone. It is deduced that the average results of $F1$ and $F3$ may be closer to the real ones, so $F13$ is empirically defined by this way. The values by $F13$ change very slowly when $M > 8$. In Fig. 4(a), $F3$ converges faster, while $F1$ and $F2$ gradually coincide to get close to $F3$. Thus, we conclude that for low-loss rectangular TCSWGs, the accurate results may be evaluated by averaging those of $F1$ and $F3$; for lossless ones, $F3$ could be directly employed.

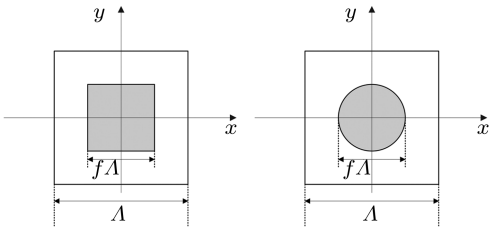


Fig. 5. Rectangular and circular shapes in a unit cell.

For circular crossed gratings, $F3$ shows better convergence, especially in Fig. 4(b), we observed that there is almost no change in R_{00} by $F3$ when $M > 8$, to which R_{00} by $F1$ and $F2$ approach slowly as M increases. The convergence of $F3$ shown in Fig. 3(b) is less better due to the absorption, but the values by $F3$ change little when $M > 10$, while those by $F1$ and $F2$ still decrease towards $F3$ in a relative larger step even when $M > 11$. Therefore, for circular TCSWGs, especially dielectric ones, $F3$ could be used to model the diffraction efficiency well; on the other hand, for low-loss ones, $F3$ could still be employed for larger M.

4. Validity of staircase approximation for TCSWGs without high absorption

In Section 3, the influence of eigenvalue functions on the convergence has been discussed, which is crucial to the accuracy and efficiency. Since staircase approximation is adopted, we should check its validity and influence on the convergence. As we have proven in Section 3 that $F3$ converges faster than the other two for circular TCSWGs without high absorption, we continue to apply it to confirm the validity of staircase approximation. Indeed, we did also calculate the cases by using $F1$ and $F2$, which are not shown in this paper, but we found $F3$ still converges faster.

The absorption at $\lambda = 0.3502$ μm and R_{00} at $\lambda = 0.8051$ μm, as M increases, for three different values of L are given in Tables 1 and 2 respectively. A careful examination reveals that the convergences with different L show not much difference. Besides, the numerical results of absorption and R_{00} converge as L increases, and the differences of them for $L = 25$ and 45 are so small that they can be neglected.

We did observe a relatively poor convergence for $\lambda = 0.3502$ μm, which is mainly attributed to the formulation of the eigenvalue functions. The slightly slower convergent rate with larger L, as shown in Tables 1 and 2, is caused by the slow convergence of Fourier expansions. With $ga1 = 0$, the larger L results in smaller duty ratio of the divided slices on the top, which should be represented with a larger M in view of mathematics.

Table 1. Absorption of TCSWGs in silicon calculated by using $F3$, the parameters are: $\lambda = 0.3502$ μm, $\Lambda = 0.15$ μm, $d = 0.35$ μm, $ga1 = 0$, $ga2 = 1$, normal incidence.

M	$L = 5$	$L = 25$	$L = 45$
2	0.8598	0.8467	0.8458
3	0.8827	0.8622	0.8613
4	0.8759	0.8658	0.8648
5	0.8666	0.8678	0.8668
6	0.8627	0.8691	0.8681
7	0.8609	0.8703	0.8691
8	0.8603	0.8712	0.8701
9	0.8604	0.8719	0.8709
10	0.8610	0.8725	0.8715
11	0.8614	0.8729	0.8721
12	0.8616	0.8733	0.8726
13	0.8616	0.8736	0.8730
14	0.8615	0.8738	0.8734

Table 2. R_{00} of TCSWGs in silicon calculated by using $F3$, the parameters are: $\lambda = 0.8051$ μm, $\Lambda = 0.15$ μm, $d = 0.35$ μm, $ga1 = 0$, $ga2 = 1$, normal incidence.

M	$L = 5$	$L = 25$	$L = 45$
2	0.0255	0.0253	0.0255
3	0.0245	0.0256	0.0258
4	0.0259	0.0254	0.0256
5	0.0259	0.0253	0.0255
6	0.0262	0.0250	0.0254
7	0.0262	0.0250	0.0253
8	0.0261	0.0249	0.0252
9	0.0261	0.0248	0.0251
10	0.0261	0.0248	0.0251
11	0.0261	0.0247	0.0250
12	0.0260	0.0246	0.0250
13	0.0260	0.0246	0.0249
14	0.0260	0.0246	0.0249

5. Comparison between the numerical and experimental results

TCSWGs reported by Kanamori *et al.* in Ref. [20], is chosen to be simulated, and the comparison is made with their experimental result. The parameters used in simulation are extracted from Ref. [20]: $\Lambda = 0.15$ μm, $d = 0.35$ μm, $ga1 = 0.1$, $ga2 = 0.95$, $L = 25$, $M = 11$, $\theta = 5°$, $\varphi = 0°$, square-latticed cone-like TCSWGs of silicon. The "$L = 25, M = 11$" are derived from the conclusions of Sections 3 and 4. To calculate the reflectance in the solar spectra, where the absorption of silicon is small, $F3$ could be used. $R_{\rm s}$ for $\psi = 90°$ and $R_{\rm p}$ for $\psi = 0°$ were computed to get $R = (R_{\rm s} + R_{\rm p})/2$. The numerical result is shown in Fig. 6. A rather good agreement is obtained with the experimental result of Fig. 3 in Ref. [20]. We observed the same local minima reside in around 400 nm and 560 nm, and the maximum at 470 nm. The deviation may be due to the difference between the simulation and the real profiles. The depths of the real TCSWGs are not perfectly the same, some of which are lower than 350 nm. Besides, the surface of the fabricated TCSWGs is rough to some extent, thus leading to further reduction in the reflectance.

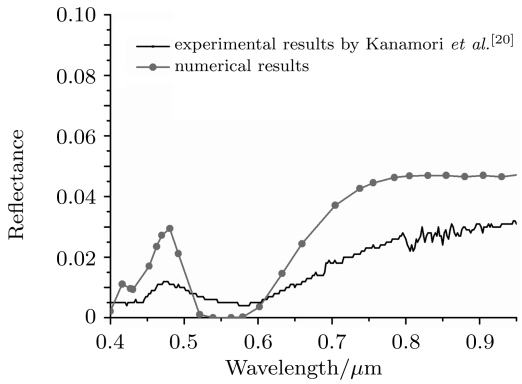


Fig. 6. Comparison between numerical and experimental results.

6. Conclusions

To study the diffraction efficiency of TCSWGs, FMM combined with staircase approximation has been established and explicitly illustrated. Three intuitive formulations of eigenvalue functions are compared with each other and discussed. For rectangular TCSWGs with small absorption, none of them show satisfactory convergence, but we found that the average value of $F1$ and $F3$ may be closer to the accurate ones. For lossless rectangular and circular TCSWGs, $F3$ is demonstrated to work well. $F3$ could be used even for low-loss circular TCSWGs, though larger M would be required accordingly. Besides, we also proved through applying $F3$ to circular non-highly-absorptive TCSWGs, that the convergence does not deteriorate and the numerical results converge with the increase in the number of slices. It is inevitable to introduce the local maxima at the edges of every divided slice for highly absorptive gratings under staircase approximation, but the problem is not so obvious in the case of small absorption, and it may be eased in lossless TCSWGs. Finally, the simulation result based on our approach is very close to the experimental one, which further proves the validity of our approach. The FMM along with staircase approximation could be used to study and optimize the antireflection characteristic of lossless or low-loss "moth-eye" structures.

Acknowledgment

The authors are grateful to Prof. Li Li-Feng at Tsinghua University for his help on understanding Li's theorem. We are also indebted to Dr. Kanamori at Tohoku University, for his provision of the experimental result of Ref. [20] and his helpful discussions.

References

[1] Moharam M G and Gaylord T K 1981 *J. Opt. Soc. Am.* **71** 811

[2] Moharam M G and Gaylord T K 1982 *J. Opt. Soc. Am.* **72** 1385

[3] Moharam M G and Gaylord T K 1986 *J. Opt. Soc. Am.* A **3** 1780

[4] Moharam M G, Grann E B, Pommet D A and Gaylord T K 1995 *J. Opt. Soc. Am.* A **12** 1068

[5] Lalanne P and Morris G M 1996 *J. Opt. Soc. Am.* A **13** 779

[6] Li L 1996 *J. Opt. Soc. Am.* A **13** 1870

[7] Zhao H J, Peng Y J, Tan J, Liao C R, Li P and Ren X X 2009 *Chin. Phys.* B **18** 5326

[8] Zhou C H, Wang L and Wang Z H 2001 *Acta Phys. Sin* **50** 1046 (in Chinese)

[9] Noponen E and Turunen J 1994 *J. Opt. Soc. Am.* A **11** 2494

[10] Li L 1997 *J. Opt. Soc. Am.* A **14** 2758

[11] Lalanne P 1997 *J. Opt. Soc. Am.* A **14** 1592

[12] Granet G and Plumey J P 2002 *J. Opt.* A: *Pure Appl. Opt.* **4** S145

[13] Popov E and Neviere M 2001 *J. Opt. Soc. Am.* A **18** 2886

[14] Li L 2003 *J. Opt.* A: *Pure Appl. Opt.* **5** 345

[15] Clapham P B and Hutley M C 1973 *Nature* **244** 281

[16] Stavenga D G, Foletti S, Palasantzas G and Arikawa K 2006 *Proc. R. Soc.* B **273** 661

[17] Boden S A and Bagnall D M 2008 *Appl. Phys. Lett.* **93** 133108

[18] Sun C H, Jiang P and Jiang B 2008 *Appl. Phys. Lett.* **92** 061112

[19] Song Y M, Bae S Y, Yu J S and Lee Y T 2009 *Opt. Lett.* **34** 1702

[20] Kanamori Y, Sasaki M and Hane K 1999 *Opt. Lett.* **24** 1422

[21] Bai B and Li L 2006 *J. Opt. Soc. Am.* A **23** 572

[22] Schuster T, Ruoff J, Kerwien N, Rafler S and Osten W 2007 *J. Opt. Soc. Am.* A **24** 2880

[23] Weiss T, Granet G, Gippius N A, Tikhodeev S G and Giessen H 2009 *Opt. Express* **17** 8051

[24] Popov E, Neviere M, Gralak B and Tayeb G 2002 *J. Opt. Soc. Am.* A **19** 33

[25] Logofatu P C 2005 *Proc. SPIE* **5972** 59720Q-1

[26] Li L 1996 *J. Opt. Soc. Am.* A **13** 1024

[27] Kim H, Lee I M and Lee B 2007 *J. Opt. Soc. Am.* A **24** 2313

[28] Moharam M G, Pommet D A, Grann E B and Gaylord T K 1995 *J. Opt. Soc. Am.* A **12** 1077

[29] Palik E D 1985 *Handbook of Optical Constants of Solids* (New York: Academy) pp. 565, 566